energies

MDPI

Article

Assessing Environmental Dynamics and Angular Influence on PV Soiling: Employing ANFIS to Mitigate Power Losses

Zahraa M. Rashak [1], Kadhim H. Hassan [1], Mustafa Al-Fartoos [2,*], Yusuf Chanchangi [2], Mohammad Hadi Mohammadi [3] and Asif Ali Tahir [3]

[1] Department of Electrical Engineering Techniques, Basrah Engineering Technical College, Southern Technical University, Basrah 61001, Iraq; zahraa.rishig@fgs.stu.edu.iq (Z.M.R.); k.hassan@stu.edu.iq (K.H.H.)
[2] Solar Energy Research Group, Environment and Sustainability Institute, Department of Engineering, University of Exeter, Penryn TR10 9FE, UK; y.n.chanchangi@exeter.ac.uk
[3] Camborne School of Mines, University of Exeter, Penryn TR10 9FE, UK; m.h.mohammadi@exeter.ac.uk (M.H.M.); a.tahir@exeter.ac.uk (A.A.T.)
* Correspondence: ma994@exeter.ac.uk

Abstract: The performance of solar photovoltaic systems is impacted by dust accumulation, raising maintenance concerns and discouraging wider adoption to accelerate decarbonization pathways. This research investigates the influence of environmental dynamics on dust accumulation based on several locations, considering weather conditions, seasonality, and angular installation variations, over a three-month period. Low-iron glass coupons were employed to collect on-site soiling from four different locations: agricultural, residential, industrial, and desert. The samples collected were characterized using scanning electron microscopy (SEM) for morphology, X-ray diffraction (XRD) for mineralogy, energy-dispersive X-ray spectroscopy (EDX) for elemental analysis, spectrophotometry for optical properties, and I–V tracing for efficiency analysis. The data were processed using ANFIS techniques to extract the maximum power point (MPP) and reduce the power losses. The results showed significant differences in the dust properties across the sites, influenced by the topography, weather conditions, and human activity. The measurements revealed a decrease in transmittance of up to 17.98%, resulting in power losses of up to 22.66% after three months. The findings highlight the necessity for tailored maintenance strategies to mitigate the impact of human activities and site-specific factors on performance. This could be employed in developing predictive models providing valuable insights for sustaining solar energy systems.

Keywords: soiling; dust accumulation; soiling properties; transmittance; PV power; tilt PV; Basra; Iraq; maximum power point

check for updates

Citation: Rashak, Z.M.; Hassan, K.H.; Al-Fartoos, M.; Chanchangi, Y.; Mohammadi, M.H.; Tahir, A.A. Assessing Environmental Dynamics and Angular Influence on PV Soiling: Employing ANFIS to Mitigate Power Losses. *Energies* **2024**, *17*, 5921. https://doi.org/10.3390/en17235921

Academic Editor: Philippe Leclère

Received: 5 November 2024
Revised: 20 November 2024
Accepted: 23 November 2024
Published: 26 November 2024

Copyright: © 2024 by the authors. Licensee MDPI, Basel, Switzerland. This article is an open access article distributed under the terms and conditions of the Creative Commons Attribution (CC BY) license (https://creativecommons.org/licenses/by/4.0/).

1. Introduction

Advances in technology have significantly improved the efficiency of energy harvesting from renewable sources, making solar energy a highly promising option. This clean and renewable source of energy is abundant in many regions, and it is estimated that Earth receives enough solar energy in just 90 min to meet the global energy demand for an entire year [1]. Despite its potential, the proportion of solar energy currently utilized remains relatively limited. However, this trend is changing rapidly, driven by global initiatives to enhance energy access, secure supply chains, and address climate change and air pollution. Extensive research is underway to investigate various aspects of solar energy utilization, with a focus on the efficiency of solar panels, which is essential for the economic sustainability of solar photovoltaic (PV) cells that convert solar energy into electricity. The efficiency of these panels is affected by multiple factors, including solar radiation, temperature, wind speed, rainfall, humidity, dew point, and cloud cover [2,3]. Therefore, understanding how these variables affect the efficiency of solar panels has become a critical research area.

Sunlight weakens as it passes through various atmospheric layers and substances due to scattering, absorption, and reflection. By the time it reaches a solar cell, only a small portion is converted into electricity due to factors like scattering, absorption, and reflection by airborne particles and surface contaminants like dust. These effects reduce the amount of sunlight available for conversion, significantly limiting the solar power generation efficiency [4]. The size, shape, roughness, and weight of particles further influence light transmission [5]. A study of the physical and chemical aspects of dust showed that the size of the dust particles in the region range from 600 nm to 10 μm, with specific minerals such as quartz, hematite, and lime, with a notable effect on glass transmittance [6–8]. Moreover, there are many research works demonstrating that dust can affect the optical transmittance of glass, which plays a crucial role in the performance of PV solar cells [9,10].

The global PV output has grown dramatically from 100 terawatt hours (TWh) in 2013 to 1300 TWh in 2022 [11]. Iraq has great potential for solar energy production. This is because Iraq receives a high intensity of solar radiation, with the annual sunny hours ranging from 3600 to 4300 h. These favorable solar conditions make Iraq well suited for generating solar power [12,13]. Hassan et al. (2021) evaluated the potential for solar energy in Iraq and the feasibility of generating electricity using a 20-megawatt solar PV power plant [12]. Faihaa Field, a 2.5 MW solar power plant in Basra, the country's first off-grid solar power facility, has successfully saved 1732 L of diesel daily since it began operations [14]. Solar power farms in dry desert regions like Basra face significant challenges due to dust buildup on the solar panels. This dust accumulation negatively impacts the power generation capacity of the solar farm [14,15]. Therefore, it is necessary to assess dust accumulation, maintain the solar panels, and find solutions to reduce its effects.

A study highlighted the importance of monitoring the dust accumulation on PV panels, emphasizing the current challenges and future approaches for tracking soiling. It assessed the existing monitoring techniques, projected market trends, and underscored the need for thousands of new soiling monitoring systems to be implemented annually [16]. The soiling rate on surfaces is not uniform as it depends on several variables. These include the local climate, the orientation of the installation, the season, the duration of exposure, and the level of human activity in the region [17]. Dust and sand deposition on PV panels can be uniform or non-uniform depending on the panel size, tilt angle, and wind velocity. While wind and rainfall are typically considered to be natural cleaners, they can sometimes worsen the soiling on panels [18]. Periods of solid and dusty winds followed by light showers can drastically negatively impact the solar system's performance. Experimental studies have demonstrated that higher wind speeds tend to increase the deposition of dust on the PV panel surfaces, which can later reduce the power output of the solar system [18–20]. Practical experiments showed that, during dust storms in Baghdad, the intensity of the solar radiation decreased by up to 54.5%, the electrical efficiency decreased by 65.58% when operating indoors, and the electrical efficiency decreased by 82.93% when operating outdoors [21].

Many studies have been conducted to investigate the accumulation effects on solar panels and the effects of atmospheric parameters and soil properties on the accumulation of soil on the PV surface, which leads to power losses and economic losses [22]. Environmental and operational factors affect solar PV performance, so it is important to explore the potential benefits of using self-cleaning and anti-reflective coatings. These coatings can improve efficiency by 11% and reduce the negative impacts of dust and humidity [23]. The deposition of dust in humid conditions forms adhesive and sticky mud on the PV cell, which worsens the situation by reducing the power generation by up to 60–70% [24]. A system using light-dependent resistors to detect dust showed a 33.76% increase in power output after cleaning [25]. A waterless method for removing dust from solar panels using electrostatic induction, aided by absorbed moisture, achieved recovery of up to 95% of the lost power output [26].

This comprehensive study aims to investigate the effect of dust accumulation on the performance and efficiency of PV panels in Basra, southern Iraq. It investigates the dust

particle size and shape in determining the efficiency of PV. A comparative analysis is undertaken regarding the effect of different environmental locations on the accumulation of dust and their subsequent effects on PV efficiency. Moreover, the study examines several factors influencing accumulation rates, including climatic conditions, panel orientation, seasonal variations, exposure duration, and human activities. Additionally, this study develops a framework for extracting the maximum power point (MPP) that could help in reducing the effect of dust accumulation on PV efficiency. The findings of this comprehensive study are expected to provide valuable insights to inform the development of tailored maintenance strategies and solutions to optimize the solar energy production in Basra or similar dust-prone environments.

2. Materials and Methods

2.1. Location and Climatic Characteristics

Basra is located in southern Iraq (30°30′30.672″ N, 47°46′49.44″ E). It is not close to the Sahara Desert but is part of the desert regions of the Arab world that have arid climates [27]. The Basra region faces severe environmental problems, such as desertification and increased salt levels in the soil, leading to land degradation [28,29]. Basra is an area rich in oil, and its soil may be contaminated with petroleum hydrocarbons because of oil processing, which has likely increased after 2003 due to increased oil extraction activities, highlighting the need to assess and monitor the environmental impacts [30]. Selecting the optimal for PV system installation is a critical determinant of its energy production. Since the favorable solar conditions in Basra and successful solar energy projects make it an ideal location for installing PV panels to harness renewable energy efficiently, and as it has high radiation levels compared to other cities in Iraq, the geographical coordinates of the city of Basra make it a suitable location for installing PV panels [14,31]. But, Basra is also considered to have a highly polluted (AQI) air quality index [32].

To fully understand the influence of weather conditions, locations, and installation positions on soiling accumulation, low-iron glass coupons 50 mm × 50 mm (length × breadth) with 4 mm thickness were placed in different locations with different positions at different weather conditions and durations in Basra. Basra covers an area of approximately 8395.85 km^2 and has diverse location environments. To cover all the different types of regions in Basra, the coupons were installed at four locations in Basra from a climatic and environmental perspective. The locations include the residential area, where a coupon was installed in Basra city center (30.488038° N, 047.831948° E); the agricultural area, where a coupon was installed in Al-Faw (30.160228° N, 048.378397° E); the industrial area, where a coupon was installed in Al-Zubair at South Refineries Company in Al-Shuaiba (30.450753° N, 047.668482° E); and the open area, where a coupon was installed in Al-Zubair (30.46765° N, 047.467922° E), as shown in Figure 1a.

The placement of the coupons significantly influences the accumulation of soiling. So, each group of coupons was placed in four positions, as indicated in Figure 1b: 1—vertical (90°); 2—tilt facing north; 3—tilt facing south (the optimal tilt of PV modules according to the location in which they are installed, as illustrated in Table 1); and 4—horizontal (0°). The coupon holder fabricated by 3D printer from (Acrylonitrile Butadiene Styrene) material. The design and material allow the jig to remain stable in extreme weather conditions, such as rain, high temperatures, and dusty winds. After their exposure period, all coupons were collected and sent to the Solar Energy Research Laboratory at the University of Exeter, Penryn Campus, UK, for detailed characterization. The transport box for the coupons was also designed and manufactured carefully to minimize movement, vibration, and the risk of breakage. Figure 1c shows the horizon and sun path generated by the PVSyst 8 software [33]. This graph represents the daily sunlight hours over the entire year at the pilot site. The insights gained from this graph are useful for assessing solar availability and potential at a given site.

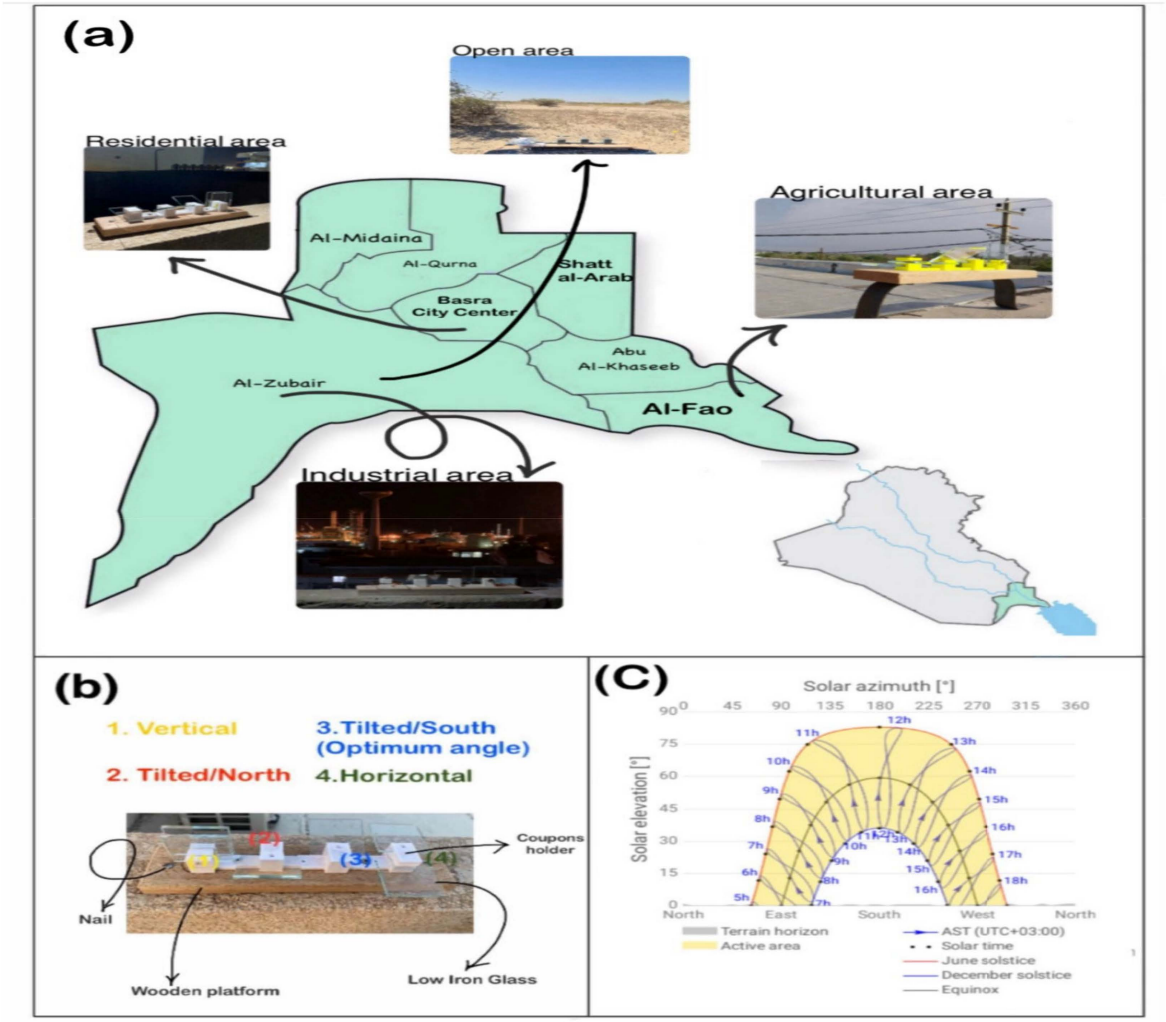


Figure 1. (**a**) Stations of glass coupons installed in different areas (agricultural, industrial, residential, and open areas), (**b**) tilt of research coupon installation (vertical, tilted, and horizontal), and (**c**) sun path and horizon line with an elaborated sketch highlighting sun availability in Basra, southern Iraq (N 30°30′30.672″, E 47°46′49.44″) [33].

Critical solar radiation data for various research sites in Basra are presented in Table 1, including information on direct average irradiation (DNI), global horizontal irradiation (GHI), diffuse horizontal irradiation (DHI), global horizontal irradiation at an optimum angle (GTI opta), tilted terrain elevation (ELE), and the optimum tilt angle for PV modules (OPTA). The optimal setup for solar panels depends on two key factors: orientation and tilt angle. In Basra Governorate, Iraq, the optimal orientation is southward as this direction ensures that the panels receive the maximum possible solar radiation when the Sun is at its highest point in the sky. Consequently, all panels were oriented south to maximize sunlight exposure. The tilt angle, which refers to the inclination of the panels relative to the horizontal plane, was determined based on the specific conditions of each location. This optimal tilt angle is essential because it directly impacts the amount of solar radiation the panels absorb, thereby influencing their efficiency and overall energy output. These data are considered for the four most important models (regions) that cover the entirety of Basra in terms of the differences in environmental and climatic conditions and human interaction. These data are essential for effective planning and design of solar initiatives in these regions as they provide crucial insights for assessing solar potential and improving the efficiency of solar systems.

Table 1. Site information in Basra, southern Iraq [33].

	locations	Direct Normal Irradiation (DNI)	Global Horizontal Irradiation (GHI)	Diffuse Horizontal Irradiation (DHI)	The Global Tilted Irradiation at an Optimum Angle (GTI Opta)	The Terrain Elevation (ELE)	Optimum Tilt of PV Modules (OPTA)
Basra city center	Residential	1895.6 kWh/m^2	2039.6 kWh/m^2	803.0 kWh/m^2	2255.3 kWh/m^2	2 m	28/180°
Al-Faw	Agricultural	1884.4 kWh/m^2	2034.5 kWh/m^2	805.4 kWh/m^2	2245.3 kWh/m^2	1 m	27/180°
Al-Zubair	Industrial	1866.2 kWh/m^2	2033.6 kWh/m^2	815.1 kWh/m^2	2246.9 kWh/m^2	9 m	28/180°
Al-Zubair	Open area (Desert)	1871.4 kWh/m^2	2038.6 kWh/m^2	816.7 kWh/m^2	2263.4 kWh/m^2	15 m	29/180°

Weather conditions, such as wind, rainfall, temperature, and humidity, play a crucial role in dirt accumulation on solar panels. Although wind and rain can act as natural cleaning mechanisms, their effectiveness depends on their intensity. For example, strong winds can dislodge loose dirt, while heavy rain can effectively remove accumulated dirt. Conversely, light winds may lack the force needed to remove dust/dirt, insufficient rainfall can exacerbate dirt by dispersing the dust and creating water spots, or high temperatures can cause dust to adhere more firmly to the panels, especially if the surface becomes hot. High temperatures combined with rain or humidity can help to create a natural cleaning cycle where rainwater helps to remove dirt and heat dries and removes it. High humidity alone does not clean panels, but, when combined with rain, it can improve cleaning efficiency. Therefore, understanding the specific weather patterns in a given area is vital for accurately predicting and mitigating the effects of contamination on solar panel performance. Figure 2 shows the average weather conditions measured in Basra during the installation period from January to March, the study period, during which the coupons were exposed to generally dry and dusty conditions with low relative humidity, infrequent rainfall, moderate wind speeds, gradually increasing temperatures, and increasing daylight hours. Cloud cover increases slightly, while solar radiation also tends to increase. Finally, the duration of coupon installation with weather changes has a significant impact on dirt accumulation. Therefore, it is necessary to know and determine the appropriate maintenance periods and also which months have the greatest impact on dirt.

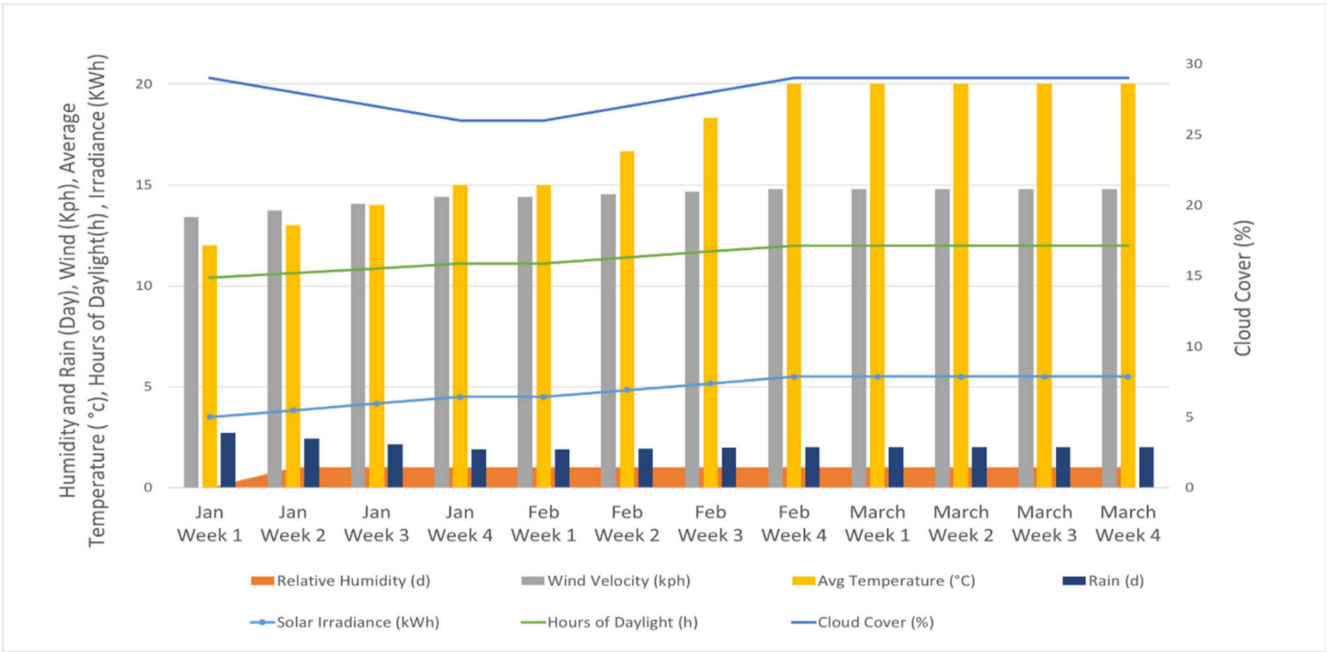


Figure 2. Average climatic conditions for Basra during the three-month installation period of January, February, and March.

2.2. Measurement of Transmittance

Optical characterization was performed to assess the transparency of the different coupon samples. The measurements were carried out using a Perkin Elmer Lambda 1050 UV/VIS/NIR spectrophotometer. To begin, a clean coupon was tested to determine the optimal transmittance level for low-iron glass. Following this, all exposed coupons underwent the same testing process, measuring transmittance levels across UV (ultraviolet), VIS (visible), and NIR (near infrared) wavelengths from 300 nm to 1200 nm. This spectrum encompasses the absorption range of all photovoltaic technologies available on the market.

The optical scanning focused on the areas of the coupon with the highest levels of accumulated substance. This was conducted because the spectrophotometer instrument required an area of around 200 square millimeters. The reasoning behind this approach was to consider the worst-case scenario. It was assumed that the areas on the heavily soiled coupon with less accumulated substance were due to natural cleaning by environmental factors like wind, rain, or gravity.

To determine the percentage difference in transmittance between the clean coupon and the coupon positioned at an angle, which helps to quantify the impact of the angular positioning on the transmittance, Equation (1) [34] was used, presented below as follows:

$$Relativechange\ (\Delta\tau_x) = \frac{(\tau_{clean} - \tau_x)}{\tau_{clean}}(\%) \quad (1)$$

where $\Delta\tau_x$ is the relative change in transmittance, τ_{clean} represents the transmittance data for a clean coupon, and τ_x represents the transmittance data for a coupon exposed to the outside atmosphere.

2.3. Mineralogical Characterizations

Mineralogical characterizations was conducted to study the morphology, elemental composition, and crystal structure of soiling particles. The Bruker D8 advanced XRD System is used to characterize the crystal structure of the accumulation of soiling particles. XT Nova Nanolab 600 scanning electron microscopy (SEM) was employed to study the nanostructure morphology of the accumulated soiling particles. Moreover, Oxford Instrument X-MAXN was used to perform energy-dispersive X-ray spectroscopy (EDX) on the accumulation of soiling particles, which enabled the chemical analysis of the elemental composition.

2.4. PV Performance Measurement

The standard PV module's performance was tested using a WACOM continuous solar simulator as illustrated in Figure 3. The WACOM Solar Simulator system setup integrates an EKO MP160 I–V tracer for data acquisition and a PC for visualization and processing. The temperature of measurement controlled at 25 °C. The irradiance level needed to be highlighted (1000 w/m^2). Initially, the standard PV module was tested without any covering surface to establish baseline performance data. Following this, each module was tested individually with a clear low-iron glass coupon. After that, the tests involved placing the soiling coupons over the standard module. The module was recalibrated after every 10 tests, and, to avoid temperature-induced voltage degradation, it was not exposed to light for long periods.

Validation of results using Equation (2) [5]:

$$SL_{Pv} = \frac{P_{max\ clean} - P_{max\ dusty}}{P_{max\ clean}} \quad (2)$$

This equation represents the PV soiling, where (SL_{PV}) is the soiling loss, ($P_{max\ clean}$) is the maximum power output of a clean module, and ($P_{max\ dusty}$) is the maximum power output of a module with soiling accumulation.

$$P_{max} = I_{max}V_{max} \quad (3)$$

This equation defines the maximum power output, where (I_{max}) is the load current that maximizes the output power and (V_{max}) is the voltage that maximizes the power output.

Adaptive Neuro-Fuzzy Inference System (ANFIS) model used to extract the maximum power point (MPP) to reduce the energy losses from soiling impact. The I–V data collected from I–V tracers at different soiling conditions were used as input data in the ANFIS model programmed by MATLAB (version 7.3). The model is trained over 100 cycles to adjust the membership functions and optimize the fuzzy rules to minimize prediction errors. After training, the MPP was identified by finding the maximum predicted power.

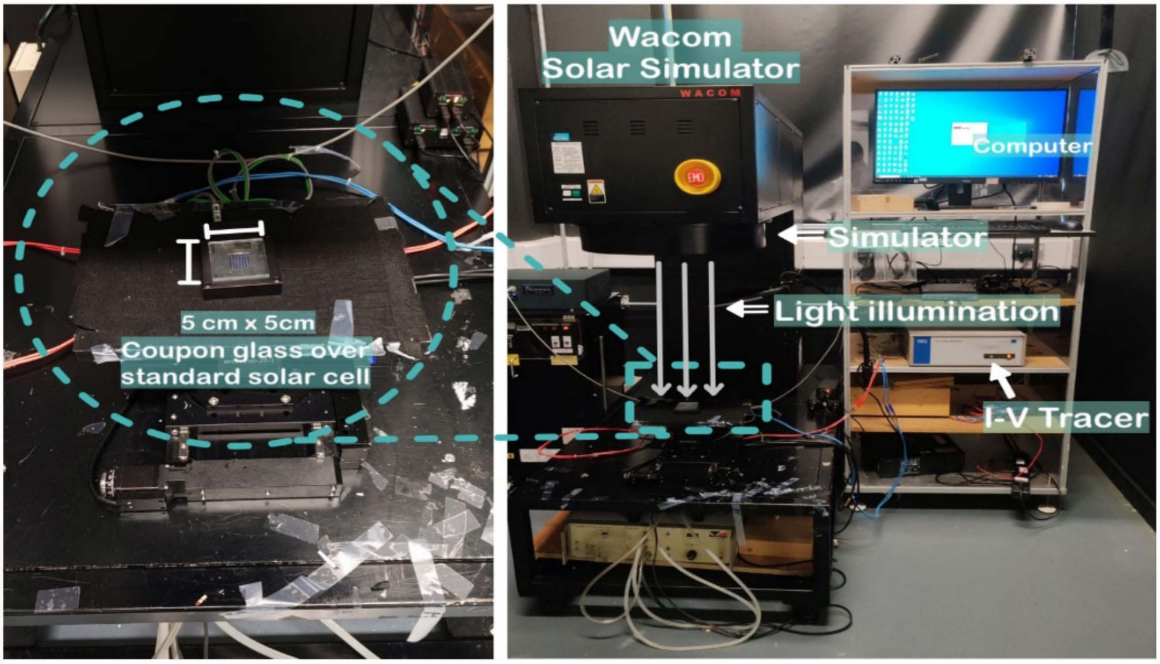


Figure 3. Standard solar simulator equipped with I–V tracer for measuring the output power of standard PV (photovoltaic) cell under standard conditions. Coupons were placed above the standard cell and under the solar simulation source, with an I–V tracer used to measure the voltage, current, and power output.

3. Results and Discussion

3.1. Particle Characterization

3.1.1. Study of Particle Size and Shape Properties

The SEM images in Figure 4 show the morphology of the particles across the study locations. In the desert (Figure 4a–c), regions of dense particle accumulation were visible alongside clear areas within the 200 µm scale (Figure 4a). The accumulated particles included coarse grains over 20 µm in size, with a crystalline structure likely originating from wind-blown sand, as well as smaller particles under 15 µm resembling mineral dust (Figure 4b). The presence of clear areas in the samples from this region suggests that natural cleaning processes, such as rainfall, played a role in reducing soiling. However, some samples revealed large particles over 5 mm adhered to the glass surface, potentially animal droppings that were not easily washed away by rain (Figure 4c). In contrast, the agricultural area (Figure 4d) exhibited low-density particle accumulation. The particles in this region appeared to be less homogeneous and formed agglomerated structures (Figure 4e), suggesting that fine dust particles accumulated in layers over time.

The industrial area (Figure 4f) displayed a denser particle accumulation than the desert and agricultural areas, with the particles demonstrating a relatively uneven size distribution. These particles exhibited a diverse, irregular shape (Figure 4g), likely due to the presence of oily materials from industrial processes that caused different types of particles to adhere to each other. The high particle concentration and irregular structure contribute to significant

light scattering and absorption, leading to a decrease in the solar energy production efficiency compared to the desert and agricultural areas. The residential area (Figure 4h) also showed high particle density, with the accumulation growing vertically, which increases the likelihood of significant transmittance losses (Figure 4i). This type of vertical accumulation is likely caused by the low wind activity in the center of the city. The high-density particle buildup, combined with larger particle sizes and vertical accumulation, contributes to increased light transmission losses and a reduction in power output.

The particle sizes from the four study locations were analyzed using a 200 μm scale for a more comprehensive overview of the accumulated particles. The average particle sizes were 13.507 μm, 23.093 μm, 10.706 μm, and 29.288 μm in the desert, agricultural, industrial, and residential areas, respectively, as shown in the supporting document (Figure 5).

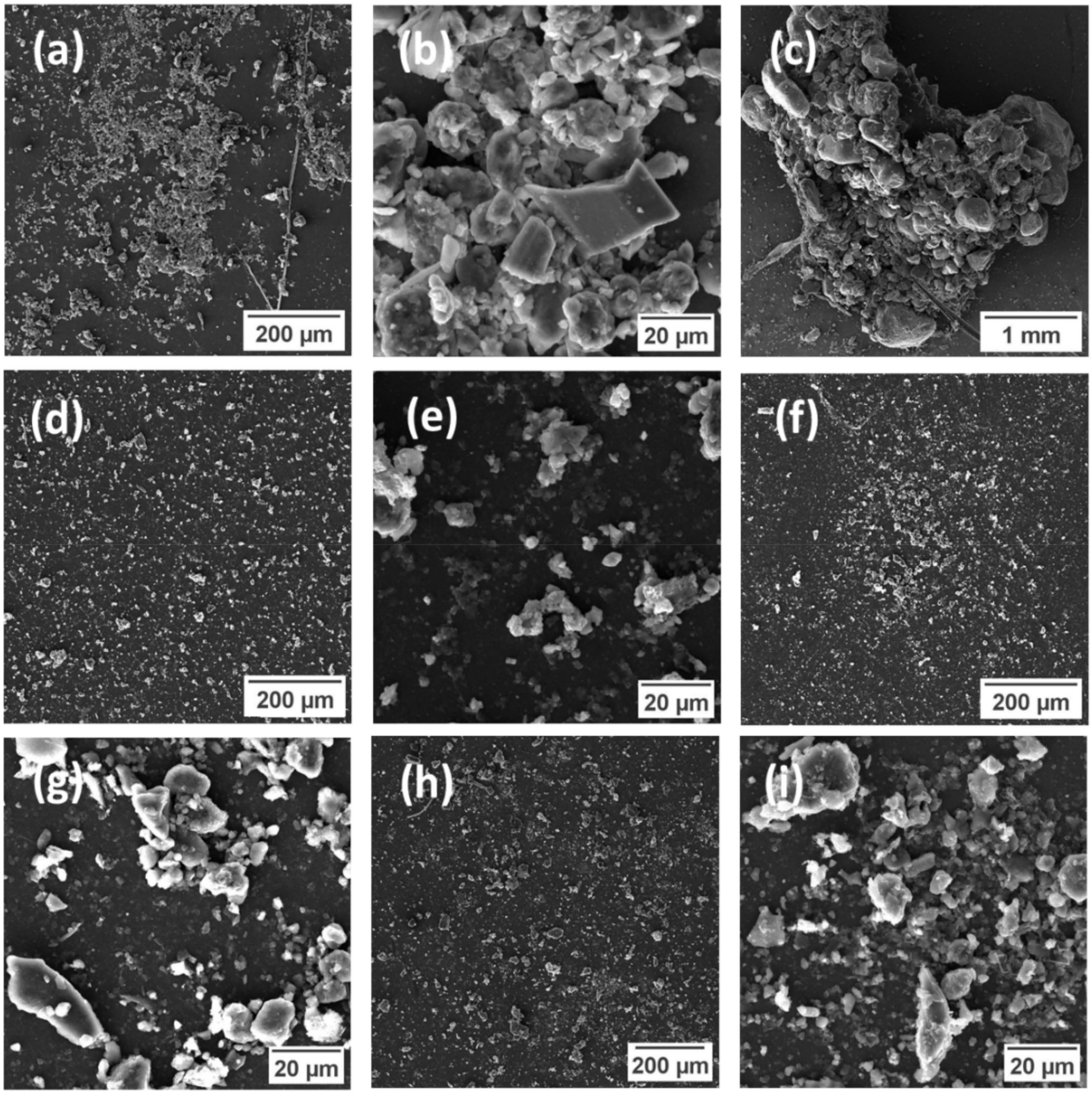


Figure 4. The SEM image study of soiling particles includes measurements for the desert at three scales (20 μm, 200 μm, and 1 mm), shown in (**a**–**c**), the agricultural area at two scales (20 μm and 200 μm) in (**d**,**e**), the industrial area at two scales (20 μm and 200 μm) in (**f**,**g**), and the residential area at two scales (20 μm and 200 μm) in (**h**,**i**).

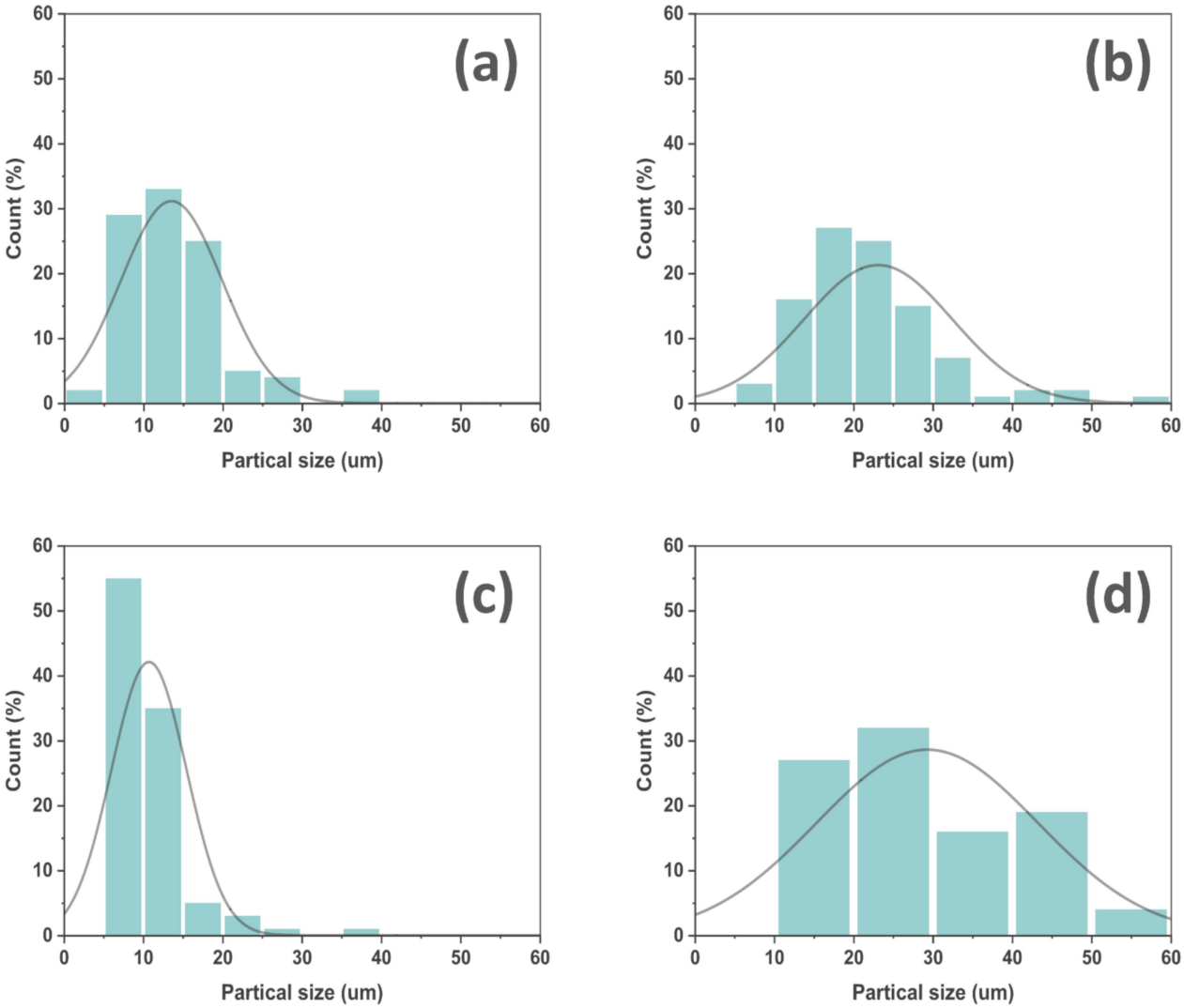


Figure 5. Image study of the soiling particle size for (**a**) desert, (**b**) agricultural, (**c**) industrial, and (**d**) residential areas. The bar chart (in cyan) represents the particle sizes within each region, as a percentage. The gray lines overlaid on the bar chart provide a visual representation of the spread of the data. The x-axis indicates particle sizes (μm), and the y-axis represents the percentage of particles.

3.1.2. Mineralogical Analysis

EDX was conducted to analyze the chemical composition of the dust accumulation in the four locations, as shown in Table 2. The differences in element weight across the desert, agricultural, industrial, and residential areas can be attributed primarily to differences in their atmospheric environments. In the desert, the sample shows a high concentration of silicon (Si), which results from the presence of sand and silicate mineral particles transported by the wind. Increasing levels of aluminum (Al) and calcium (Ca) are also observed as these are common elements in desert soils and rocks [35]. The agricultural area shows a higher concentration of silicon (Si), which can be attributed to the presence of soil particles and sand grains transported airborne from the surrounding farmlands, as established earlier in [36], and layer materials such as clays that have an alumino-silicate structure. The higher concentration of sodium (Na) in this area can be attributed to using sodium-containing fertilizers and/or the influence of saline soil conditions due to the irrigation practices [37]. Elevated levels of potassium (K) and calcium (Ca) are also observed, reflecting the presence of the fertilizers used in the agricultural practices [38].

Table 2. Chemical compositions of EDX for desert, agricultural, industrial, and residential areas.

Area	**Desert**										
Sample	O	Si	Al	Na	Ca	Mg	Fe	K	Sn	S	
Atomic weight percentage (%)	48	27.1	6.9	3.7	3.6	3.3	2.5	2	1.6	1.2	
Area	Agricultural										
Sample	O	Si	Ca	Na	Fe	Al	Mg	S	Sn	K	Cl
Atomic weight percentage (%)	51.8	18.1	9.7	5.9	4	3.6	3	1.6	1	0.9	0.4
Area	Residential										
Sample	O	Si	Ca	Al	S	Mg	K	Na	Fe	Cl	
Atomic weight percentage (%)	58.6	11.9	7.7	6.5	5.6	2.7	2.6	1.9	1.6	1.5	
Area	Industrial										
Sample	O	Ca	Si	Fe	Al	Mg	Ti	Na	K	Mo	S
Atomic weight percentage (%)	49.9	21	13.8	5.1	4.3	2.3	1.3	0.9	0.8	0.8	0.7

The sample from the industrial area shows a high concentration of iron (Fe), likely due to airborne particles from activities such as infrastructure corrosion, metal processing, construction, transportation, waste management, and other industrial processes involving iron-based materials commonly found in oil refineries. The relatively high levels of titanium (Ti), molybdenum (Mo), and calcium (Ca) in this area, compared to others, may be linked to specific industrial activities such as alloy production, manufacturing, cement and construction materials, steel and metalworking, and the use of catalysts containing these elements in oil refining processes. The presence of elevated levels of sulfur (S) can be attributed to crude oil processing, which typically includes these elements [39]. The coupon from the residential area shows an increased concentration of aluminum (Al), which is associated with the presence of suspended particulates from construction materials and demolitions such as facades or rooftops. The high proportions of sodium (Na) and chlorine (Cl) can be attributed to the salts suspended due to the surface evaporation of a salty lake in the area, as well as emissions from vehicles, domestic wastewater, restaurants, and other commercial establishments [40].

3.1.3. Crystalline Structure Analysis

To better understand the elemental composition and crystalline structure of the accumulated deposits, an X-ray diffraction (XRD) analysis was conducted on soil samples collected from soiling coupons placed in four locations: desert, agricultural, industrial, and residential areas. This technique identifies crystalline structures, primary mineral phases, and the presence of amorphous materials, which is essential for understanding the sources and dynamics of the particulate matter in these environments.

Figure 6 shows the XRD pattern of the soiling removed from the coupons in the four areas of the research. It reveals several distinct peaks corresponding to a specific element or compound in the soils covered by the coupons. The peaks are labeled with the corresponding elements, mainly Na, Mg, Al, Si, O, K, Ca, C, H, and Fe. The chemical formulas of the most probable minerals observed in the XRD patterns of all four coupons include quartz [SiO_2], calcite [$CaCO_3$], albite [$NaAlSi_3O_8$], muscovite [$KAl_2(AlSi_3O_{10})(OH)_2$], and pigeonite [$(Ca, Mg, Fe)_2Si_2O_6$]. Based on the following studies, quartz exhibits high transmittance in the visible spectrum, often exceeding 90% due to its crystalline structure and low absorption coefficients [41], but calcite is known for its notable birefringence, which influences its transmittance properties and causes variations in light transmission depending on the polarization state. Typically, calcite transmits about 75–85% of the visible light, with its performance affected by the crystal orientation [42]. Albite also has relatively high transmittance, comparable to quartz, although impurities and structural defects can impact its performance [43], and muscovite, a type of mica, has lower transmittance than quartz and calcite, generally ranging from 50 to 70%. Its transparency varies with thick-

ness [42]. Pigeonite ((Ca, Mg, Fe)$_2$Si$_2$O$_6$) typically exhibits lower transmittance than the other minerals, often falling below 50% [44]. The XRD results matched the EDX findings, where quartz, calcite, and albite were all recorded in four different areas.

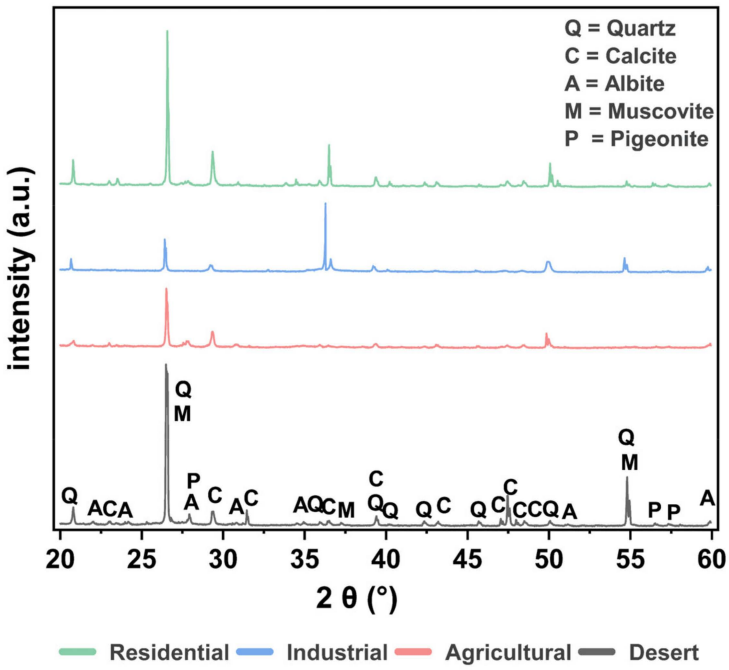


Figure 6. XRD study of dust collected from soiling coupons in four different areas.

The highest peak in the samples was quartz, indicating a dominating material. The peaks in some areas represent different minerals and elements. A simpler XRD pattern is displayed in the desert, with the main peaks corresponding to Si and Na. This is consistent with the expected composition of desert dust, typically dominated by saline soil. In addition to Si, the agriculture coupon has a significant presence of sodium-based compounds, likely from fertilizers or irrigation water. The industrial soil exhibits a very sharp and intense peak for Fe, indicating a high concentration of iron-based compounds. Additionally, the industrial sample shows several other distinct peaks, including those for Ca and Si, suggesting a more complex elemental composition than the other locations. The residential sample shows a strong peak for Q; this indicates a substantial presence of quartz in the soiling coupons compared to the other minerals.

3.2. Transmittance Losses

3.2.1. Transmittance Reduction Due to Soiling Accumulation in a Residential Area at Various Times

The average transmittance losses due to dust accumulation have been measured in a residential area at different exposure times, as shown in Figure 7. The results show that the clean coupon has a transmittance of about 91%. Moreover, Equation (1) was used to calculate the transmittance losses per coupon for the wavelength at 850 nm (the power generation peak for the standard solar cell), as illustrated in Figure 8.

The lowest transmittance reduction was observed for a vertically positioned coupon, about 5.04% during a 10-day exposure period, while the highest decrease was observed for the north-facing tilted coupon, about 8.47%, and the optimal coupon, 6.18%. When the exposure period increased to one month, the transmittance reduction for all the coupons became more apparent. The vertical coupon experienced the lowest reduction, reaching about 7.02%, while the highest noticeable decrease for an optimum-angle coupon was about 10.6%. During a two-month exposure period, the transmittance reduction continued to increase. The vertical direction maintained the lowest transmittance reduction, about

9.79%, while the optimal coupon showed 16.8%. The highest decline in transmittance was at around 17.76% for the horizontal direction. The data show that transmittance reduction increases with longer exposure periods. After three months, the vertical coupon also showed the lowest decrease, about 12.83%, while the optimum tilt coupon showed 17.33% if the highest decrease was about 17.98% for the horizontal coupon.

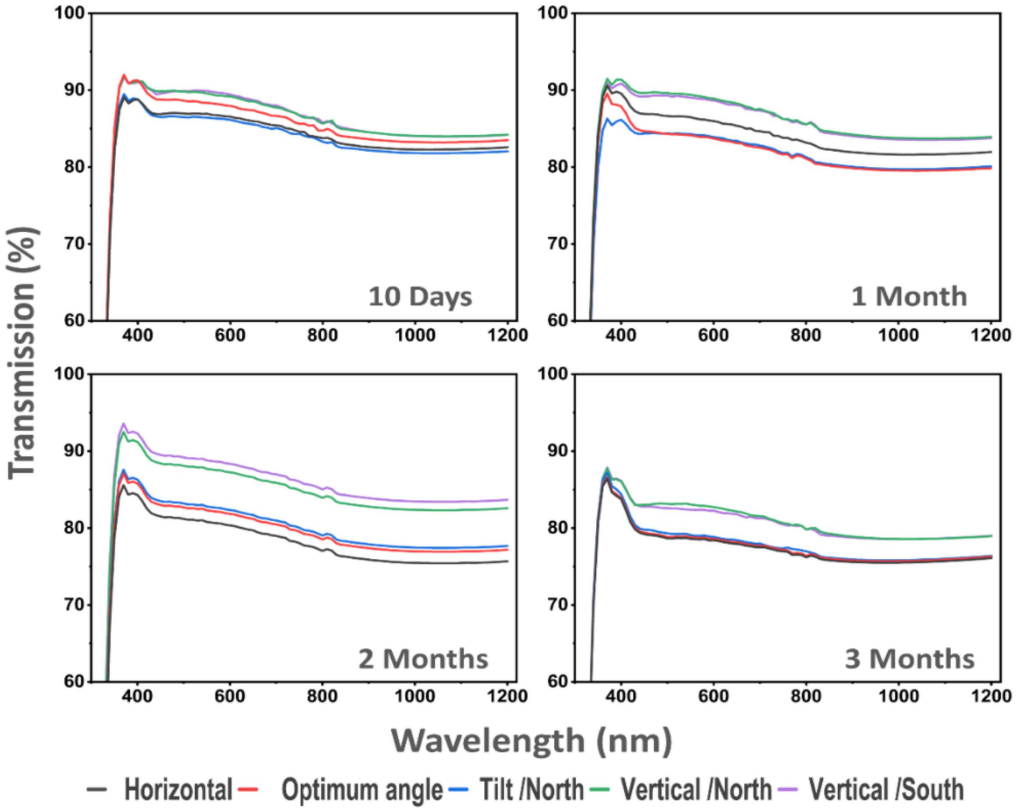


Figure 7. Optical transmittance of the coupons was measured at different tilt angles (horizontal, two opposing 28° tilt angles, and two vertical coupons in opposite directions) over various exposure durations (10 days, 1 month, 2 months, and 3 months).

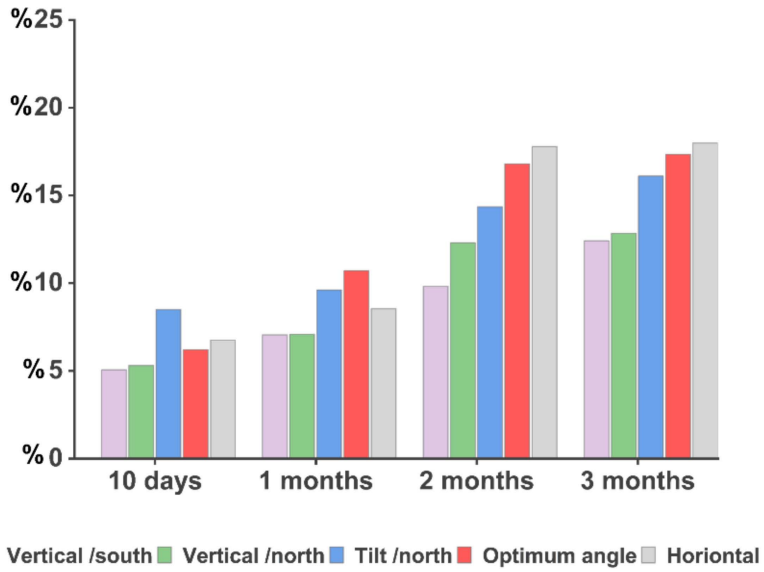


Figure 8. Average transmittance losses measured for different orientations at four different exposure times.

The results indicate that the tilted coupons (optimal angle) at 28 degrees for the residential area, as shown in Table 1, accumulate more soiling than the vertical and slightly less than horizontal ones. This is due to increased exposure to soiling particles and the gravity effect, especially when there is no high wind effect in the residential area.

3.2.2. Transmittance Reduction Due to Soiling Accumulation in Four Different Regions

The average transmittance losses in the four study environment areas at 3 months of exposure duration are shown in Figure 9. Figure 10 illustrates the calculated transmittance losses per coupon for the wavelength at 850 nm. Across the different regions, the desert area experienced the lowest losses at 6% for the vertical orientation, with the highest losses at 11.59% for the horizontal orientation. The optimal angle showed slightly lower losses than the horizontal, at about 8.38%. In the agricultural area, the lowest transmittance losses were also for the vertical orientation at 6.6%, while the highest were at 13.68% for the horizontal, very close to the optimal angle's losses of 13.47%.

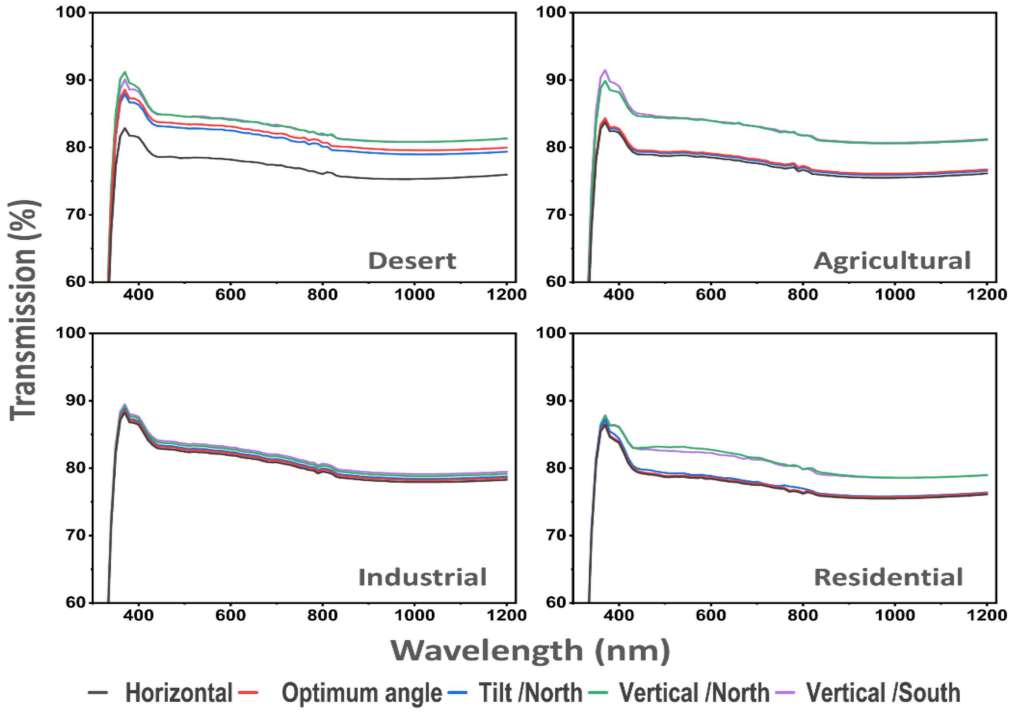


Figure 9. Optical transmittance of the coupons was measured at different tilt angles (horizontal, two opposing 28° tilt angles, and two vertical coupons in opposite directions) across four regions: desert, agricultural, industrial, and residential areas at the same installed period for three months.

The industrial area showed a comparable trend in transmittance losses, with 12.13% for the vertical coupon, 12.56% for the optimal angle, and 12.99% for the horizontal orientation. In the residential area, higher losses were observed in all four orientations compared to the other areas, with 12.4% for the vertical, 17.33% for the optimal angle, and 17.98% for the horizontal. These results demonstrate that surface orientation and environmental conditions significantly impact dirt accumulation.

It is noted that the desert area shows slightly lower losses than the agricultural area, and both have the lowest transmittance losses compared to the other regions. This is attributed to their open environments, where wind and rain help to reduce dirt accumulation. In contrast, the industrial area has higher transmittance losses due to the easy adhesion of soil caused by sticky chemical pollution. Finally, the residential area exhibits the highest transmittance losses, likely due to its confined space, which limits the wind's natural cleaning effect, along with high pollution from cars, homes, construction, and evaporation residues from nearby water sources.

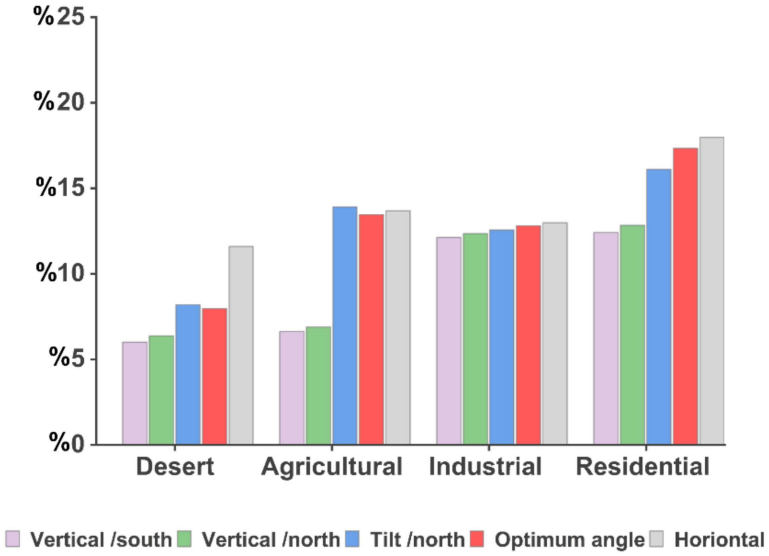


Figure 10. Average transmittance losses measured for different orientations across four different regions installed for three months.

When comparing the optimal tilt angle with the other orientations in relation to the soiling accumulation, the results indicate that the optimal orientation, designed to maximize solar radiation exposure, may not necessarily produce the highest power output due to soiling. Vertical orientations can experience lower transmittance losses depending on the surrounding environment, suggesting that PV windows integrated into buildings could be successful in such areas due to their vertical installation.

3.3. P–V Power Losses

3.3.1. P–V Performance Reduction Due to Soiling Accumulation in a Residential Area at Various Times

Figure 11 illustrates the I–V (current–voltage) curves, while Figure 12 presents the P–V (power–voltage) curves for the coupons installed in the residential area at different tilt angles and installation durations. The initial measurement was taken with the 'standard' coupon, which was clean and free of dust, showing the highest performance in the tests.

By using Equation (2) to calculate the power output losses per coupon, as shown in Figure 13, after 10 days, a noticeable decrease in power output was observed across all the coupons, with the losses reaching 9.96% for the coupon at the optimal angle compared to the clean reference. This rapid degradation in performance due to the initial dust and dirt accumulation continued over one month, resulting in a further decline in power output and losses reaching up to 13.75%. This trend persisted, with the losses increasing to 19.05% after two months and further escalating to 22.66% after three months of accumulation, highlighting the significant impact of soiling accumulation on PV module performance.

The study underscores the importance of proper tilt and orientation in reducing the effect of soiling on PV module performance. The vertical coupon showed the lowest power output losses, likely due to the appropriate incidence angle and enhanced self-cleaning from wind and rain. The optimal angle coupon followed this. In contrast, the horizontal coupon showed the highest power output losses and the worst loss performance, around 25.38% more than the vertical coupon, due to the increased particle accumulation over time. In another study, comparing the energy losses for the optimal angle, we found that they were higher than the energy losses when the coupon was vertical. The energy losses for the vertical coupon over ten days were approximately only 1.86%, calculated relative to a clean coupon. Similarly, the losses for the coupon over a month were approximately 3.6%; over two months, they were about 4.92%; and, finally, over three months, they were 16.09%.

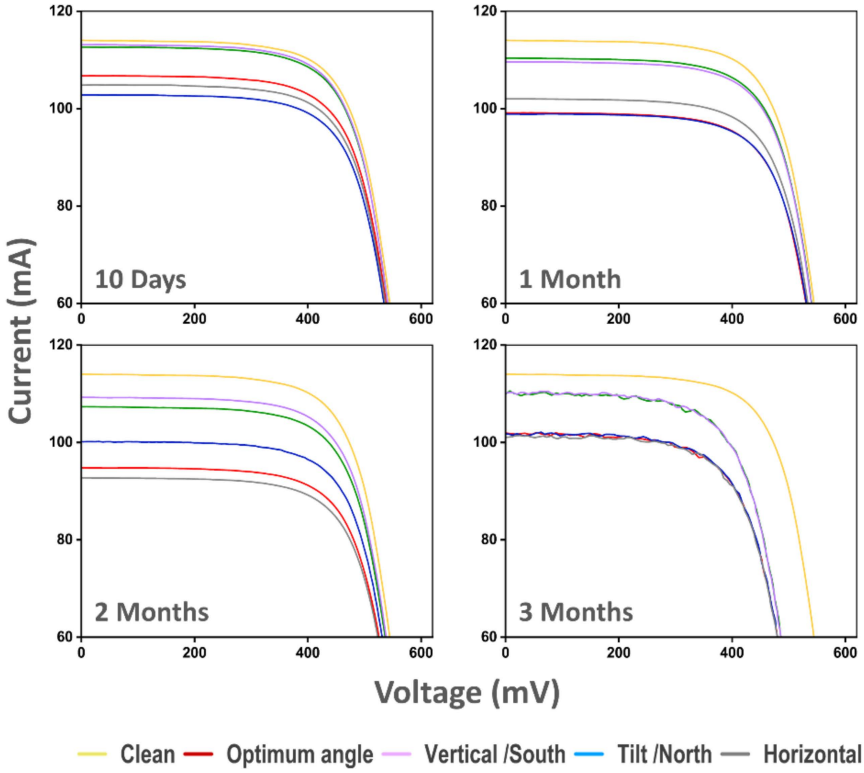


Figure 11. I–V curves were measured at different tilt angles (horizontal, two opposing 28° tilt angles, and two vertical coupons in opposite directions) over various exposure durations (10 days, 1 month, 2 months, and 3 months).

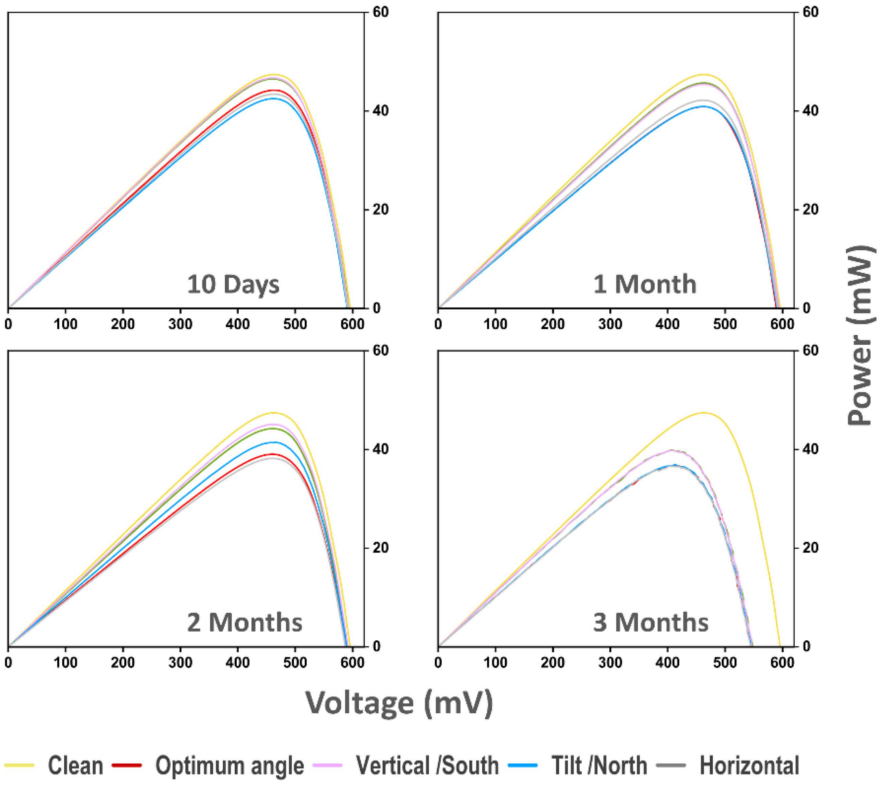


Figure 12. P–V curves at different tilt angles (horizontal, two opposing 28° tilt angles, and two vertical coupons in opposite directions) over various exposure durations (10 days, 1 month, 2 months, and 3 months).

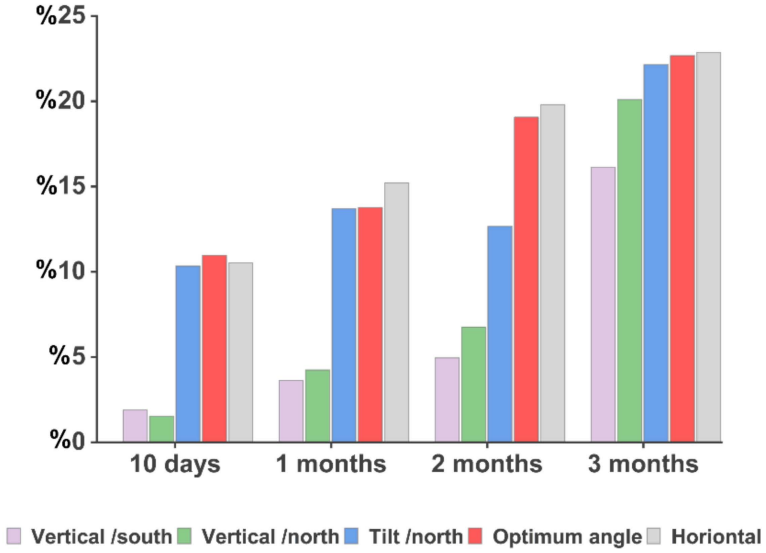


Figure 13. Power output losses recorded from coupons at different tilt angles in residential areas at four different exposure times.

3.3.2. P–V Performance Reduction Due to Soiling Accumulation in Four Different Positions

The highest power output for the coupons at different tilt angles and regions was recorded using the I–V tracer. Figure 14 shows the I–V (current–voltage) curves, while Figure 15 describes the P–V (power–voltage) curves. Moreover, Figure 16 shows the power output losses measured for the coupons exposed to atmospheric conditions over three months at various mounting angles across four distinct areas.

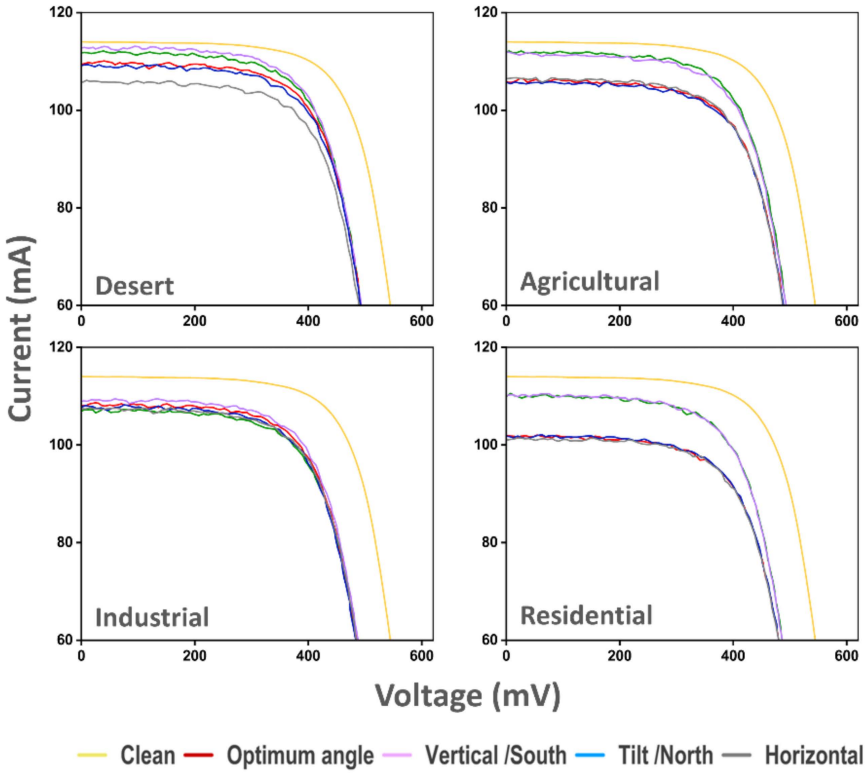


Figure 14. I–V curves were measured at different tilt angles (horizontal, two opposing 28° tilt angles, and two vertical coupons in opposite directions) at different regions: desert, agricultural, industrial, and residential areas in the same installation period of three months.

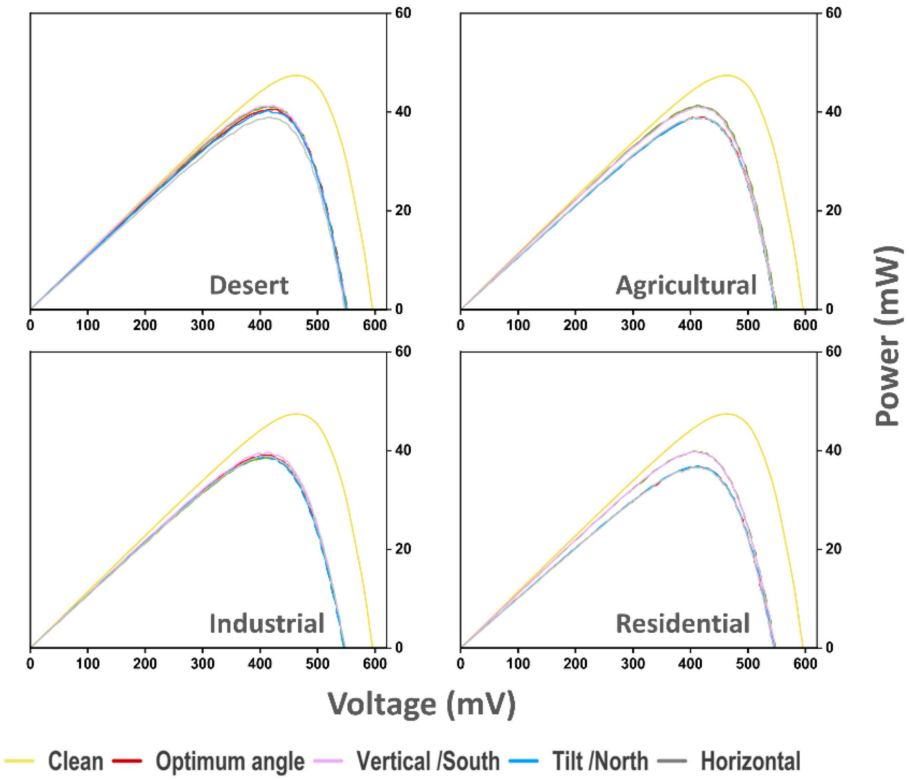


Figure 15. P–V curves at different tilt angles (horizontal, two opposing 28° tilt angles, and two vertical coupons in opposite directions) at different regions: desert, agricultural, industrial, and residential areas in the same installation period of three months.

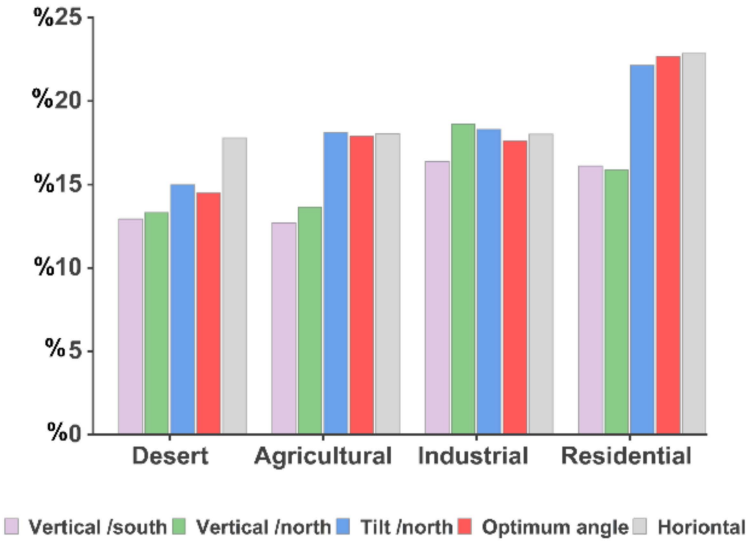


Figure 16. Power output losses recorded at different tilt angles (horizontal, two opposing 28° tilt angles, and two vertical coupons in opposite directions) at different regions: desert, agricultural, industrial, and residential areas during the same installation period of three months.

The power losses of the vertical coupons were recorded as follows: desert (12.48%), agricultural (12.68%), industrial (16.5%), and residential (16.09%). For the optimal tilt angle, the losses were desert (14.5%), agricultural (17.8%), industrial (17.6%), and residential (22.6%). The horizontal coupon losses were desert (17.8%), agricultural (18%), industrial (18.5%), and residential (22.66%). The findings reveal a consistent trend across all the areas: the horizontal samples incurred the highest power losses over time, followed by

the tilted samples, whereas the vertical samples exhibited the lowest losses. The horizontal configuration, being the most exposed to particle buildup, suffered the greatest performance degradation. The highest power losses were recorded in the residential area, while the agricultural and industrial areas showed similar losses, with the industrial area experiencing slightly higher energy losses. The desert area exhibited the lowest energy losses. These findings closely align with the transmittance data, confirming the correlation between power losses and light transmittance. The maintenance requirements for solar panels vary significantly depending on the location, prevailing weather conditions, and the duration of exposure. For example, the residential areas showed slightly less power loss after one month (13.75%) compared to the desert environment after three months (14.5%). Solar panels that are not cleaned regularly can experience a substantial reduction in energy production due to the accumulation of contaminants. Additionally, as shown in Figure 17, the power losses increased rapidly between two and three months of accumulation in the agricultural, industrial, and residential areas. However, the power losses increased slightly in the desert due to self-cleaning by the weather compared to the other areas. These findings highlight the importance of considering the local atmospheric conditions and seasonal variations when evaluating solar panel systems' performance and maintenance requirements.

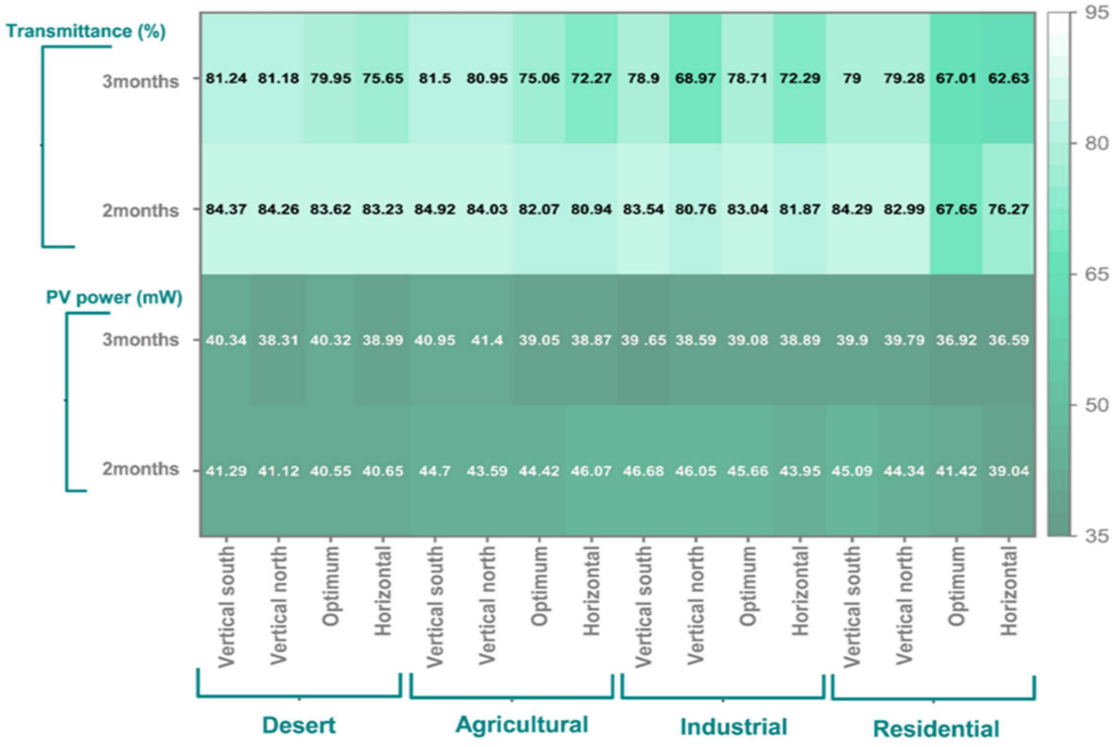


Figure 17. Shows the extracted maximum power point (MPP) and transmittance measured for coupons exposed at four orientations across four locations after two and three months.

4. An ANFIS Approach to Maximizing Power Production

The use of an ANFIS for tracking the MPP in the context of accumulated soiling on PV panels aims to enhance the energy production by optimizing the efficiency of solar panel systems. The system works by modeling the complex nonlinear relationships between input variables such as current and voltage and soiling, thereby providing accurate predictions. The ANFIS also adapts to varying environmental conditions, such as different levels of soiling and shading, ensuring optimal performance [45]. Through real-time monitoring and the ability to predict power output, the system can make immediate adjustments to maintain the MPP. Furthermore, the ANFIS supports predictive maintenance by analyzing the impact

of soiling, aiding in improving maintenance and cleaning schedules. It provides valuable insights for operators and maintenance personnel, enabling informed decision-making regarding system upkeep. By reducing energy losses, the ANFIS supports sustainable practices, contributing to greater reliance on renewable energy sources.

Data measured using an I–V curve tracer were processed in MATLAB to calculate and extract the MPP under shading conditions caused by dirt accumulation on the coupons over installation periods of two and three months, as shown in Figure 17. The simulation results closely align with the manual measurements taken during the three-month installation period but show an improvement in power output. For instance, the power output at the optimal angle in the desert was 40.01 mW, while the value extracted using the ANFIS was 40.32 mW. Additionally, the power output in the desert area improved by 0.77% with the use of the ANFIS, while, in the industrial area, it increased from 39 mW to 39.08 mW. Applying the ANFIS consistently enhanced the output power by more than 0.6% in the residential areas.

An ANFIS significantly enhances PV system performance by optimizing the maximum power point tracking (MPPT) under soiling and shading conditions, leading to consistent power output improvements. With real-time adjustments, an ANFIS saves power, translating to substantial cumulative energy savings over time. It supports predictive maintenance and improves efficiency. It is a powerful tool for sustainable solar energy management and maximizing renewable energy system performance, particularly in challenging environmental conditions. This integrated methodology represents a rigorous approach to verifying the accuracy and reliability of data analysis, as shown in Figure 18. This ratio indicates the difference between manual measurements and computer modeling to optimize solar energy systems by understanding the specific energy loss patterns across different land use types and installation configurations. Figure 18 demonstrates the significant impact of optimizing the tilt angles on energy extraction using the MATLAB model for MPPT. The results reveal that the optimum tilt angle provides noticeable enhancements in power output, with improvements of 0.28% in the agricultural area, 0.77% in the desert area, 0.6% in the residential area, and 0.2% in the industrial area. Notably, the vertical south orientation achieves the highest power enhancement, reaching up to 1.33% in the agricultural area, highlighting its effectiveness in specific environments and tilt angles. In contrast, the horizontal orientation shows the lowest improvement, with the power enhancements ranging from 0.01% to 0.02% across all the areas. These findings underscore that the use of an ANFIS for MPPT enhances energy extraction, even in challenging environments, contributing to the overall sustainability and reliability of renewable energy systems.

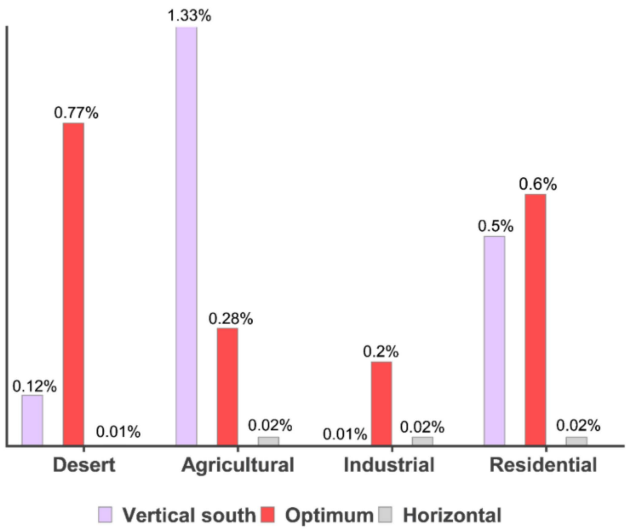


Figure 18. Understand and optimize solar panel performance by assessing the discrepancies between real-world measurements and computational modeling.

5. Conclusions

This comprehensive study, conducted in Basra, southern Iraq, explored how factors such as location, installation angle, duration, and weather conditions affect the accumulation of dust and dirt on solar panels. By examining various regions, including agricultural, residential, industrial, and open desert areas, over a three-month period, the research provided valuable insights into the factors influencing the solar panel performance and maintenance needs. The study found that the regional environmental conditions significantly impact the accumulation of dirt and dust, altering the size, quantity, and composition of the collected particles. Among the studied locations, the residential areas exhibited the highest energy losses due to soiling, followed by the industrial, agricultural, and desert areas, with the agricultural regions experiencing the least losses. Panel orientation also played a critical role in the accumulation process; the horizontal installations had the highest energy losses due to larger deposition areas, while the vertical panels benefitted from gravity and wind, which facilitated self-cleaning. This suggests that, while optimal angles are designed to maximize solar radiation exposure, they may still suffer from increased soiling, leading to lower power output.

The characteristics of the accumulated particles, including their size, shape, and quantity, were found to directly impact the amount of light reaching the solar panels, consequently affecting the energy production. The weather conditions, such as rainfall and wind speed, also played a vital role in the accumulation and natural cleaning processes, with wind and rain helping to reduce soiling in some conditions. The maintenance needs were shown to vary significantly depending on the location, weather, and duration of exposure; for instance, the residential areas experienced slightly less power loss after one month (13.75%) compared to the desert environment after three months (14.5%).

Finally, the study highlighted that using maximum power point (MPP) extraction methods, such as an ANFIS, provides more accurate predictions of the solar panel performance under various conditions and enhances the power output. These findings emphasize the need for tailored maintenance strategies and site-specific approaches to enhance the efficiency and lifespan of solar energy systems, particularly in regions prone to heavy soiling and environmental variability.

Author Contributions: Conceptualization, Z.M.R., K.H.H., Y.C. and M.A.-F.; methodology, Z.M.R., M.A.-F. and Y.C.; software, Z.M.R.; validation, Z.M.R., K.H.H. and Y.C.; formal analysis, Z.M.R., M.A.-F., Y.C., M.H.M. and A.A.T.; investigation, Z.M.R.; resources, A.A.T.; data curation, Z.M.R., Y.C. and M.H.M.; writing—original draft preparation, Z.M.R.; writing—review and editing, Z.M.R., K.H.H., Y.C., M.H.M., M.A.-F. and A.A.T.; visualization, Z.M.R., K.H.H. and Y.C.; supervision, K.H.H. and A.A.T.; project administration, A.A.T. and K.H.H. All authors have read and agreed to the published version of the manuscript.

Funding: This research was funded by Engineering and Physical Sciences Research Council (EPSRC) under research grant number EP/T025875/1.

Data Availability Statement: All data supporting the findings of this study are included within the article. Additional data or materials can be made available upon reasonable request to the corresponding author.

Acknowledgments: The author A.A.T. would like to thank Engineering and Physical Sciences Research Council (EPSRC) for financial support under research grant number EP/T025875/1. Z.M.R. would like to express sincere gratitude to the Solar Research Group at the Environment and Sustainability Institute, University of Exeter, for hosting her as a visiting student and providing laboratory facilities to conduct experiments.

Conflicts of Interest: The authors declare that they have no known competing financial interests or personal relationships that could have appeared to influence the work reported in this paper.

References

1. Philibert, C. *Solar Energy Perspectives*; OECD: Minneapolis, MN, USA, 2011. [CrossRef]
2. Guangul, F.M.; Chala, G.T. Solar Energy as Renewable Energy Source: SWOT Analysis. In Proceedings of the 2019 4th MEC International Conference on Big Data and Smart City, Muscat, Oman, 15–16 January 2019; IEEE: New York, NY, USA, 2019; pp. 1–5. [CrossRef]
3. Sarmah, P.; Das, D.; Saikia, M.; Kumar, V.; Yadav, S.K.; Paramasivam, P.; Dhanasekaran, S. Comprehensive Analysis of Solar Panel Performance and Correlations with Meteorological Parameters. *ACS Omega* **2023**, *8*, 47897–47904. [CrossRef] [PubMed]
4. Al Garni, H.Z. The Impact of Soiling on PV Module Performance in Saudi Arabia. *Energies* **2022**, *15*, 8033. [CrossRef]
5. Chanchangi, Y.N.; Ghosh, A.; Sundaram, S.; Mallick, T.K. An analytical indoor experimental study on the effect of soiling on PV, focusing on dust properties and PV surface material. *Sol. Energy* **2020**, *203*, 46–68. [CrossRef]
6. Bazarbayev, R.; Zhou, B.; Allaniyazov, A.; Zeng, G.; Mamedov, D.; Ivanitskaya, E.; Wei, Q.; Qian, H.; Yakubov, K.; Ghali, M.; et al. Physical and chemical properties of dust in the Pre-Aral region of Uzbekistan. *Environ. Sci. Pollut. Res.* **2022**, *29*, 40893–40902. [CrossRef]
7. Yu, F.; Nie, W.; Zhou, W.; Yuan, M.; Yan, J.; Hua, Y.; Bao, Q.; Niu, W. Performance evaluation of Mn-Ce/cordierite catalyst modified by green surfactant to remove NOx in underground mines at low temperatures. *J. Environ. Chem. Eng.* **2021**, *9*, 106499. [CrossRef]
8. Nie, W.; Liu, C.; Hua, Y.; Bao, Q.; Niu, W.; Jiang, C. Study on PM diffusion and distribution of trackless rubber-tyred vehicle under different driving conditions in underground coal mining environment. *Environ. Sci. Pollut. Res.* **2023**, *30*, 99484–99500. [CrossRef]
9. Abdellatif, S.O.; Amr, L.; Kirah, K.; Ghali, H.A. Experimental Studies for Glass Light Transmission Degradation in Solar Cells Due to Dust Accumulation Using Effective Optical Scattering Parameters and Machine Learning Algorithm. *IEEE J. Photovolt.* **2023**, *13*, 158–164. [CrossRef]
10. Rudnicka, M.; Klugmann-Radziemska, E. The Issue of Shading Photovoltaic Installation Caused by Dust Accumulation on the Glass Surface. *Ecol. Chem. Eng. S* **2021**, *28*, 173–182. [CrossRef]
11. Renewables. 2023. Available online: https://www.iea.org/energy-system/renewables/solar-pv (accessed on 30 June 2024).
12. Hassan, Q.; Hafedh, S.A.; Hasan, A.; Jaszczur, M. Evaluation of energy generation in Iraqi territory by solar photovoltaic power plants with a capacity of 20 MW. *Energy Harvest. Syst.* **2022**, *9*, 97–111. [CrossRef]
13. Ali, T.E.; Abdala, M.A.; Al-Khaykan, A.; Alwahab, D.A.; Counsell, C.M. Energy generation by crystalline silicon photovoltaic network per meter square in Iraq. *Int. J. Electr. Comput. Eng.* **2023**, *13*, 3606. [CrossRef]
14. Ma, R.; Liu, J. The First Off-Grid Solar Power Plant in Iraq. In Proceedings of the Gas & Oil Technology Showcase and Conference, Dubai, United Arab Emirates, 13–15 March 2023; SPE: Kuala Lumpur, Malaysia, 2023. [CrossRef]
15. Aïssa, B.; Isaifan, R.J.; Figgis, B.W.; Abdallah, A.A.; Bachour, D.; Perez-Astudillo, D.; Sanfilippo, A.; Lopez-Garcia, J.; Benito, V.B. A Comprehensive Review of a Decade of Field PV Soiling Assessment in QEERI's Outdoor Test Facility in Qatar: Learned Lessons and Recommendations. *Energies* **2023**, *16*, 5224. [CrossRef]
16. Bessa, J.G.; Micheli, L.; Almonacid, F.; Fernández, E.F. Monitoring photovoltaic soiling: Assessment; challenges, and perspectives of current and potential strategies. *iScience* **2021**, *24*, 102165. [CrossRef] [PubMed]
17. Chanchangi, Y.N.; Ghosh, A.; Sundaram, S.; Mallick, T.K. Dust and PV Performance in Nigeria: A review. *Renew. Sustain. Energy Rev.* **2020**, *121*, 109704. [CrossRef]
18. Memiche, M.; Bouzian, C.; Benzahia, A.; Moussi, A. Effects of dust, soiling, aging, and weather conditions on photovoltaic system performances in a Saharan environment—Case study in Algeria. *Glob. Energy Interconnect.* **2020**, *3*, 60–67. [CrossRef]
19. Li, X.; Wang, J.; Liu, Y.; Ma, X. Effect of photovoltaic panel electric field on the wind speed required for dust removal from the panels. *Chin. Phys. B* **2023**, *32*, 084103. [CrossRef]
20. Dagher, M.M.; Kandil, H.A. Computational prediction of dust deposition on solar panels. *Environ. Sci. Pollut. Res.* **2022**, *30*, 12545–12557. [CrossRef]
21. Chaichan, M.T.; Kazem, H.A.; Al-Waeli, A.H.A.; Sopian, K.; Fayad, M.A.; Alawee, W.H.; Dhahad, H.A.; Isahak, W.N.R.W.; Al-Amiery, A.A. Sand and Dust Storms' Impact on the Efficiency of the Photovoltaic Modules Installed in Baghdad: A Review Study with an Empirical Investigation. *Energies* **2023**, *16*, 3938. [CrossRef]
22. Borah, P.; Micheli, L.; Sarmah, N. Analysis of Soiling Loss in Photovoltaic Modules: A Review of the Impact of Atmospheric Parameters, Soil Properties, and Mitigation Approaches. *Sustainability* **2023**, *15*, 16669. [CrossRef]
23. Rajbahadur, Y.N.K.; Kumar, A.; Negi, S.; Kar, S. Evaluation of hydrophobic/hydrophilic and antireflective coatings for photovoltaic panels. *J. Coat. Technol. Res.* **2024**, *21*, 1–38. [CrossRef]
24. Hasan, K.; Yousuf, S.B.; Tushar, M.S.H.K.; Das, B.K.; Das, P.; Islam, M.S. Effects of different environmental and operational factors on the PV performance: A comprehensive review. *Energy Sci. Eng.* **2022**, *10*, 656–675. [CrossRef]
25. Asoh, D.A.; Awangum, N.N. Low-Cost Automated PV Panel Dust Cleaning System for Rural Communities. *Smart Grid Renew. Energy* **2022**, *13*, 173–199. [CrossRef]
26. Panat, S.; Varanasi, K.K. Electrostatic dust removal using adsorbed moisture–assisted charge induction for sustainable operation of solar panels. *Sci. Adv.* **2022**, *8*, eabm0078. [CrossRef] [PubMed]
27. Jabbar, M.T.; Zhou, J. Environmental degradation assessment in arid areas: A case study from Basra Province, southern Iraq. *Environ. Earth Sci.* **2013**, *70*, 2203–2214. [CrossRef]

28. Kounta, H.O.; Nezli, I.E.; Hacini, M.; Al Sultan, S.H. The Use of Remote Sensing and GIS for the Mapping of Diachronic Evolution from Wetlands to the Arid Regions. In *Recent Advances in Environmental Science from the Euro-Mediterranean and Surrounding Regions. EMCEI 2017*; Springer: Cham, Switzerland, 2018; pp. 1775–1778. [CrossRef]
29. Rashak, Z.; Hassan, K. The Impact of Soiling on Photovoltaic Performance in Iraq: Review. *Basrah J. Eng. Sci.* **2024**, *24*, 79–87. [CrossRef]
30. Al-Qadir, S.A.; Al-Ali, A.; Soltan, B. Monitoring Soil Contamination by Hydrocarbons and Heavy Metals in Parts of Basra Southern Iraq Using Remote Sensing and GIS Techniques. *Iraqi Geol. J.* **2023**, *56*, 29–42. [CrossRef]
31. Sakran, N.B.; Najim, S.I. Study the hybrid PV/wind systems in Basrah city. *Int. J. Curr. Eng. Technol.* **2019**, *9*, 350–356. [CrossRef]
32. Air Quality in Basra. 2024. Available online: https://air.plumelabs.com/air-quality-in-Basra-pTm (accessed on 30 June 2024).
33. Technical Report of Basra-Iraq, Global Solar Atlas. 2024. Available online: https://globalsolaratlas.info/map?c=11.523088,8.173828,3 (accessed on 14 May 2024).
34. Chanchangi, Y.N.; Ghosh, A.; Sundaram, S.; Mallick, T.K. Angular dependencies of soiling loss on photovoltaic performance in Nigeria. *Sol. Energy* **2021**, *225*, 108–121. [CrossRef]
35. Zhang, Y.; Mahowald, N.; Scanza, R.A.; Journet, E.; Desboeufs, K.; Albani, S.; Kok, J.F.; Zhuang, G.; Chen, Y.; Cohen, D.D.; et al. Modeling the global emission, transport and deposition of trace elements associated with mineral dust. *Biogeosciences* **2015**, *12*, 5771–5792. [CrossRef]
36. Barão, L.; Teixeira, R.; Vandevenne, F.; Ronchi, B.; Unzué-Belmonte, D.; Struyf, E. Silicon Mobilization in Soils: The Broader Impact of Land Use. *Silicon* **2020**, *12*, 1529–1538. [CrossRef]
37. Omar, M.M.; Massawe, B.H.J.; Shitindi, M.J.; Pedersen, O.; Meliyo, J.L.; Fue, K.G. Assessment of salt-affected soil in selected rice irrigation schemes in Tanzania: Understanding salt types for optimizing management approaches. *Front. Soil Sci.* **2024**, *4*, 1372838. [CrossRef]
38. Skorbiłowicz, M.; Skorbiłowicz, E. Content of Calcium, Magnesium, Sodium and Potassium in the Street Dust from the Area of Białystok (Poland). *J. Ecol. Eng.* **2019**, *20*, 125–131. [CrossRef]
39. Mokhtarzadeh, Z.; Keshavarzi, B.; Moore, F.; Marsan, F.A.; Padoan, E. Potentially toxic elements in the Middle East oldest oil refinery zone soils: Source apportionment, speciation, bioaccessibility and human health risk assessment. *Environ. Sci. Pollut. Res.* **2020**, *27*, 40573–40591. [CrossRef] [PubMed]
40. Abdelaal, A.; Abbas, E.A.; Beheary, M.S. Assessment of dust major ions and suspended heavy metal contents in atmospheric particulate matter of Port Said city, Egypt. *Arab. J. Geosci.* **2021**, *14*, 1419. [CrossRef]
41. Alrowaili, Z.A.; Eke, C.; Olarinoye, I.O.; Sriwunkum, C.; Tonguc, B.T.; Al-Buriahi, M.S. Radiation transmittance of the optical SiO_2-based glass system. *Optik* **2022**, *273*, 170385. [CrossRef]
42. Gong, Y.; Wang, Y.; Zhao, H.; Zeng, J.; Chang, L.; Li, T.; Li, X. Analysis of transmittance of micro-nano structure. In *Eighth Symposium on Novel Photoelectronic Detection Technology and Applications*; Zhu, S., Yu, Q., Su, J., Chen, L., Chu, J., Eds.; SPIE: Bellingham, WA, USA, 2022; Volume 12169, p. 338. [CrossRef]
43. Tian, J.; Philpot, W. Spectral Transmittance of a Translucent Sand Sample with Directional Illumination. *IEEE Trans. Geosci. Remote Sens.* **2018**, *56*, 4307–4317. [CrossRef]
44. Shahpaski, M.; Sapaico, L.R.; Süsstrunk, S. Comparative analysis of transmittance measurement geometries and apparatus. *Electron. Imaging* **2019**, *31*, 477-1–477-7. [CrossRef]
45. Biswal, P.; Pati, A.K. A Novel ANFIS Method for Detection of Maximum Power Point of Photovoltaic System. In Proceedings of the 2023 International Conference on Communication, Circuits, and Systems, Bhubaneswar, India, 26–28 May 2023; IEEE: New York, NY, USA, 2023; pp. 1–6. [CrossRef]

Disclaimer/Publisher's Note: The statements, opinions and data contained in all publications are solely those of the individual author(s) and contributor(s) and not of MDPI and/or the editor(s). MDPI and/or the editor(s) disclaim responsibility for any injury to people or property resulting from any ideas, methods, instructions or products referred to in the content.